Desalination and Water Treatment
www.deswater.com

doi: 10.5004/dwt.2023.30131

315 (2023) 227–240
December

Adsorption of Rhodamine B dye onto iodo-polyurethane foam: kinetics and thermodynamic study

Z.M. Saigl*, O.A. Aljuaid

Department of Chemistry, Faculty of Science, King Abdulaziz University, P.O. Box: 80203, Jeddah 21589, Saudi Arabia, emails: zsaigl@kau.edu.sa/zeinabsaigl@hotmail.com (Z.M. Saigl), Ohud-Aljuaid@hotmail.com/ Ohood-Aljuaid@hotmail.com (O.A. Aljuaid)

Received 30 May 2023; Accepted 8 November 2023

ABSTRACT

Even today, public health and water resources pollution issues by dyes are still the attention of researchers. Rhodamine B (RhB) is a highly toxic dye classified as carcinogenic and toxic. Among separation techniques, adsorption is used to treat polluted samples effectively. For the present study, iodo-polyurethane foam (I-PUF) was studied and tested as a solid-phase extractor for RhB adsorption. The adsorption of RhB onto I-PUF from aqueous media reached equilibrium at pH ≈ 3 in 30 min. The kinetics was evaluated through different non-linear kinetic models (Lagergren's pseudo-first-order, pseudo-second-order, Avrami and Elovich). The results indicated that the adsorption of RhB followed pseudo-second-order kinetic (R^2 = 0.9999). Additionally, the adsorption mechanism was evaluated by intraparticle diffusion models (Weber–Morris, Reichenberg and Bangham). Adsorption isotherms were examined by non-linear isotherm (Langmuir and Freundlich) models. The results indicated that the adsorption of RhB onto I-PUF was controlled by film diffusion and intraparticle diffusion. The maximum adsorption capacity of I-PUF was equal to 22.032 mg·g^{-1}. The thermodynamic parameters were calculated. The negative values of ΔH (–31.488 J·mol^{-1}) proved the exothermic nature of RhB adsorption onto I-PUF. The value of ΔS was –37.223 J·mol^{-1}·K^{-1}. The negative value of ΔG (–19.9316 kJ·mol^{-1} at 298 K) indicates the spontaneous nature of adsorption. As a result, the I-PUF efficiency has been demonstrated, and it was considered a suitable adsorbent for RhB adsorption.

Keywords: Rhodamine B; Iodo-polyurethane; Non-linear kinetic; Thermodynamic

1. Introduction

Rhodamine B (RhB) is a synthetic dye, fluorescent with a reddish violet colour and classified as a derivative of xanthene dye derivatives. The scientists Cérésole, then Homdka and Boedeker first synthesized RhB in 1887 and 1888. It is the most used cationic dye and the most toxic among the xanthene family dyes. The chemical formula and the molecular weight of RhB are $C_{28}H_{31}N_2O_3Cl$ and 479 g·mol^{-1}, respectively. RhB is a highly water-soluble, chemically stable, and non-biodegradable dye. The photic absorbance of RhB is approximately shown at wavelength 554 nm [1,2]. RhB has been widely employed in many fields, including textile colourants, paints, dye lasers, stamp pad inks, plastic, leather, fluorescent labelling, fireworks, and the leather industry [3,4]. Due to their characteristic optical properties, RhB is used as a tracer agent to determine the rate and direction of the flowing water. Also, it is employed as a fluorescence tracer agent in biochemical research [4,5]. Medical studies have proven that RhB is carcinogenic and neurotoxic [6,7]. When humans are exposed to RhB, it irritates the skin, brain, and eyes, causing headaches, vomiting, nausea, difficulty breathing, and chest pain, resulting in allergy, asthma, carcinogenicity, and chronic poisoning [7–9]. Moreover,

* Corresponding author.

according to the published report from Toronto Research Chemicals (Toronto, Canada), the LC_{50} value amounted to 887 mg·kg^{-1}. Lethal concentration (LC_{50}) is the concentration of the chemicals required to kill 50% of the test samples [10]. A toxicity test was performed on fish, where the value of LC_{50} was 83.9 mg·L^{-1} [11]. Besides, a recently published study in 2021 studied ecotoxicity for RhB and Rhodamine WT. The results concluded that RhB was more toxic than Rhodamine WT. Also, RhB concentrations must not exceed 14 μg·L^{-1} in freshwater for continuous discharges and 140 μg·L^{-1} intermittent discharges or may form a risk for freshwater aquatic life [12].

On the other hand, RhB dye cannot be allowed in foodstuffs intended for human consumption, cosmetics, and the pharmaceutical industry. Nevertheless, RhB has been found illegally used as a food colourant in foodstuff and cosmetics. The cause of using it as an illegal additive in foodstuffs and cosmetics can be attributed to fraudulent purposes to increase sales, improve effectively the extrinsic of the products, its low cost and colourfastness [13–15]. Therefore, it being highly toxic and formatting a severe threat to public health, the European Food Safety Administration (EFSA) published a regulation involving banning RhB dye from use in food and categorizing it as an illegal additive in foodstuff (commission regulation (EU)) [16]. Also, RhB was prohibited in hair products under commission regulation (EU) [17,18]. Moreover, RhB usage as a colouring agent in cosmetics and drugs has been prevented [18,19] and classified as a carcinogen by the Food & Drug Administration (FDA) [20].

Therefore, to protect public health and water resources from pollution with RhB, several chemicals, physical and biological techniques such as solid phase extraction [13], oxidation processes [21] and degradation by microbes [22] were used to treat the polluted samples. Among all the varied methods, solid–phase extraction is still gaining the attention of researchers due to its high efficiency, simplicity, low cost, and low production of hazardous waste [23,24]. Over the last few years, the adsorbents were used to remove RhB from polluted samples, such as activated carbon [25], graphene oxide [26], metal–organic framework [27] and biomass adsorbents (banana peels) [28]. However, most of these adsorbents have limitations that severely impede their practical utilization, such as high operating costs, complicated work steps, reduced adsorption rate and low selectivity. Therefore, porous adsorbents attract great research interest due to their high thermal and chemical stability, low cost, excellent adsorption capacity, high efficiency, and easy recyclability [29–31].

Polyurethane foam (PUF) is a linear polymer with three-dimensional pore structures and the chemical formula $C_{27}H_{36}N_2O_{10}$. It was manufactured by a reaction between polyols and isocyanates, known as a polyaddition reaction. PUF is considered one of the most used in the polymer family. It has been exhaustively studied thanks to its unique features and properties, such as lightweight, chemical and thermal resistance, flexibility and low cost. Besides the properties mentioned above, the PUF demonstrated its high efficiency as a solid phase extractor (adsorbent) to various dyes and other organic/inorganic pollutants [29,32–34]. In some cases, the researchers resort to a few chemical modalities to modify PUF before its usage to enhance the separation efficiency and improve selectiveness, such as magnetic nanocomposites [35], clay nanotubes [36] and chitosan [37]. However, these modalities suffer complicated application procedures, high cost and time consumption. Therefore, there is a scientific tendency to evolve the modification methods to be simple, inexpensive and have high separation efficiency [38,39].

Consequently, in this study, (i) PUF was modified through sequential and simplified steps based on the Sandmeyer reaction by the reaction between potassium iodide and the diazo group ($-N^+\equiv N$) of the PUF. Hence, the diazonium salt formed was substituted by iodide ions to form iodo-polyurethane foam (I-PUF) [40]. (ii) I-PUF efficiency was investigated for RhB adsorption by an experimental batch procedure. Besides, (iii) the thermodynamic, kinetic and isotherm models were optimized.

2. Experimental set-up

2.1. Reagents and materials

All chemicals used were of analytical reagent grade quality and were used without further purification unless stated otherwise. All solutions were prepared with deionized water. The glassware was cleaned with acetone and rinsed with deionized water before use. A stock solution of RhB (100 mg·L^{-1}) was prepared by dissolving the desired weight of RhB ($C_{28}H_{31}ClN_2O_3$) (479.02 g·mol^{-1}), (M/s Fluka, Buchs, Switzerland) in deionized water (100 mL). More diluted solutions (5–50 mg·L^{-1}) were prepared by suitable dilution of the stock solution of RhB with deionized water. Nitric acid (0.5 mol·L^{-1}) was used to adjust the pH of solutions during the extraction process (pH 3 ± 0.1). White sheets of commercially available open-cell polyurethane foam were purchased at the local market in Jeddah, Saudi Arabia. PUF cubes of approximately 1 cm^3 were clipped from the sheet. PUF was washed with HCl (10% v/v) followed by distilled water until the wash solutions were free from chloride ions. Then, PUF cubes were washed with acetone to remove organic contaminants and dried in an oven at 80°C for 2 h [41].

2.2. Apparatuses

All measuring of the absorbance of the RhB before and after extraction with the I-PUF was achieved by the ultraviolet-visible spectrophotometer Agilent (M/s model 8453, Germany) in the range between (180–800 nm) with a 10 mm quartz cell. The functional groups of PUF, I-PUF and RhB-I-PUF were detected by Fourier-transform infrared spectroscopy (FTIR spectrum 100, M/s PerkinElmer precisely, United States) in the range of (400–4,000) cm^{-1}. The surface morphology of PUF and I-PUF was investigated using a scanning electron microscope (SEM) (M/s Joel JSM-7600, Japan). A thermostatically controlled shaker (M/s GFL-1083 model, Germany) with a shacking rate of (10–250 rpm) was used in batch adsorption experiments for RhB by I-PUF solid-phase extractor. A foam weight was determined by a digitally sensitive balance (M/s A&P-110L, Japan) with four decimal numbers. Deionized water was gained from the Milli-Q Plus system (M/s Millipore, Bedford, MA, USA) and was used to prepare all the experiments. The pH of solutions was measured by Bibby Scientific Ltd., model 3510 pH meter (M/s Jenway, U.K.).

2.3. Recommended methodology

2.3.1. Preparation of I-PUF

The preparation of I-PUF was described by Moawed et al. [40]. Briefly, (5.0 ± 0.1 g) of PUF was cut into small cubes and soaked in 500 mL of HCl solution (2 mol·L^{-1}) for 24 h. According to the Sandmeyer reaction, the reaction must be achieved in two conditions to form diazonium salt: (i) the reaction occurs at 0°C, and (ii) an abundant quantity of HCl solution [42]. The PUF cubes were put in an ice bath at 0°C, and then drops of 100 mL of $NaNO_2$ solution (2 mol·L^{-1}) were added slowly with continual stirring to ensure the formation of a diazonium salt. After that, the diazo group was substituted by KI solution (50 mL, 1 mol·L^{-1}) to produce I-PUF.

The colour of the sorbent was changed from yellow to brown. Finally, the sorbent was washed with distilled water and ethanol solution. The foam cubes were dried in air and stored in a dark bottle.

2.3.2. Batch adsorption procedure

A conical flask of 250 mL contained I-PUF (0.1 ± 0.02 g) and a 50 mL known concentration of RhB dye. The solution was adjusted at the desired pH by diluted the HNO_3 solution. The solution was shaken for 1-h at 25°C ± 0.1°C by a mechanical shaker. To study the kinetics adsorption of RhB by I-PUF, 0.1 g of I-PUF was added to a 250 mL conical flask containing 5 mg·L^{-1} of RhB solution. The adsorption isotherms were studied by varying the initial RhB concentration (3–40 mg·L^{-1}). The solution was adjusted at the desired pH by diluted the HNO_3 solutions. Experiments were performed at 0 to 60 min by placing the flask on a shaker at 25°C. The thermodynamics of RhB adsorption were investigated with a 250 mL glass conical flask containing 0.1 g of I-PUF and 5 mg·L^{-1} of RhB solution. The solution was adjusted at the desired pH by diluted HNO_3 solutions. Experiments were performed at five temperatures (285, 297, 307, 313 and 333 K) by placing the glass vials on a temperature-controlled shaker. The concentrations of RhB were measured by ultraviolet-visible spectrophotometer.

3. Results and discussion

3.1. Morphology of iodo-polyurethane I-PUF

The surface morphology of PUF and I-PUF were studied employing a SEM, as shown in Fig. 1A and B. In Fig. 1A the surface morphology of PUF was smooth, with no pores. In contrast, after the modification of PUF by iodine atoms, the I-PUF surface was jagged, with lots of pores, as shown in Fig. 1B. The adsorbent porosity increase offers a suitable surface for pollutants adsorption and facilitates interaction between the adsorbent and pollutants [43]. The functional groups of PUF, I-PUF and I-PUF-RhB were determined by FTIR. The isocyanate and urethane groups (–NCO, –O–CO–NH) bands have appeared at 2,172.56 and 1,075 cm^{-1}, respectively, as shown in Fig. 2A. In Fig. 2B and D, the band at 546.70 cm^{-1} can be attributed to the C-I. The disappearance of the isocyanate group band confirms that the amine groups turned into diazonium form and then were substituted by iodine atoms [43]. In Fig. 2C, after RhB adsorption, the broadband that appeared at 3,294 cm^{-1} can be attributed to the OH from RhB.

3.2. Retention profile of RhB dye from aqueous solution onto I-PUF

3.2.1. Effect of pH on adsorption of RhB dye onto I-PUF

The pH represents one of the most variable parameters that strongly influence the retention step of the analyte. The pH effect on the adsorption of RhB onto I-PUF using the batch mode is shown in Fig. 4A. The retention profile of RhB from aqueous solutions onto I-PUF was studied at a wide range of pH (1–10). The maximum extraction of RhB percentage onto the solid phase extractor reached at pH ≈ 3 ± 0.2 and markedly decreased on increasing the solution pH, as shown in Fig. 4A. The high adsorption at pH ≈ 3 ± 0.2 can be attributed to the change in RhB nature in different solution media that forms other ionic species due to the change in pH of the solution. Fig. 3 shows the different ionic species of RhB. On the other hand, the point zero charge (pH_{pzc}) is the pH in which the adsorbent's surface carries the zero value (pH_{pzc} = 0). The pH_{pzc} has a significant role in ionizing functional groups and their interaction with target RhB

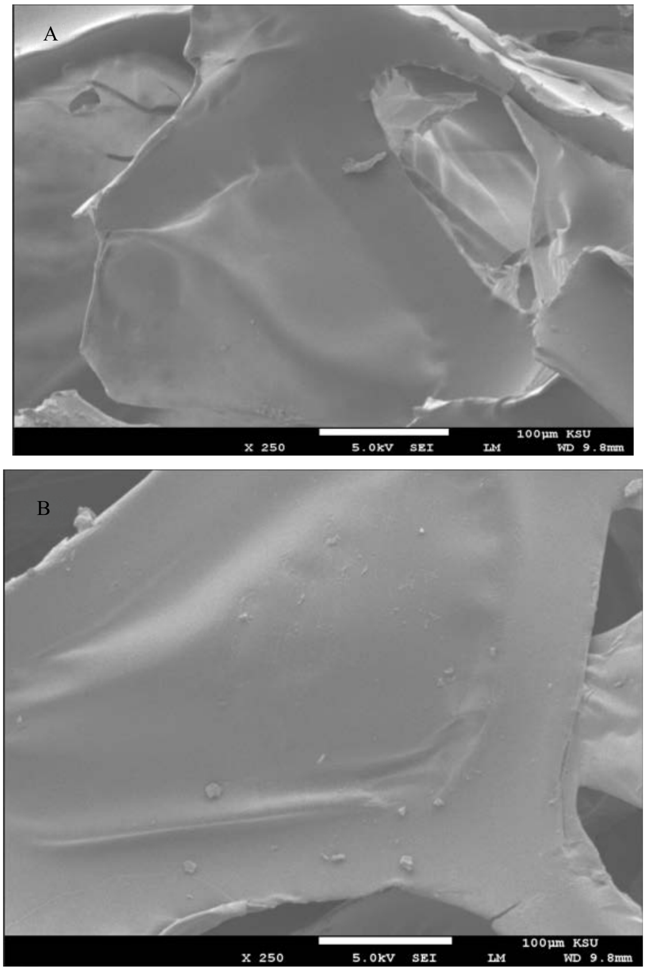

Fig. 1. Scanning electron microscope images of PUF (A) and of I-PUF (B) at 100 μm and 250 X, respectively.

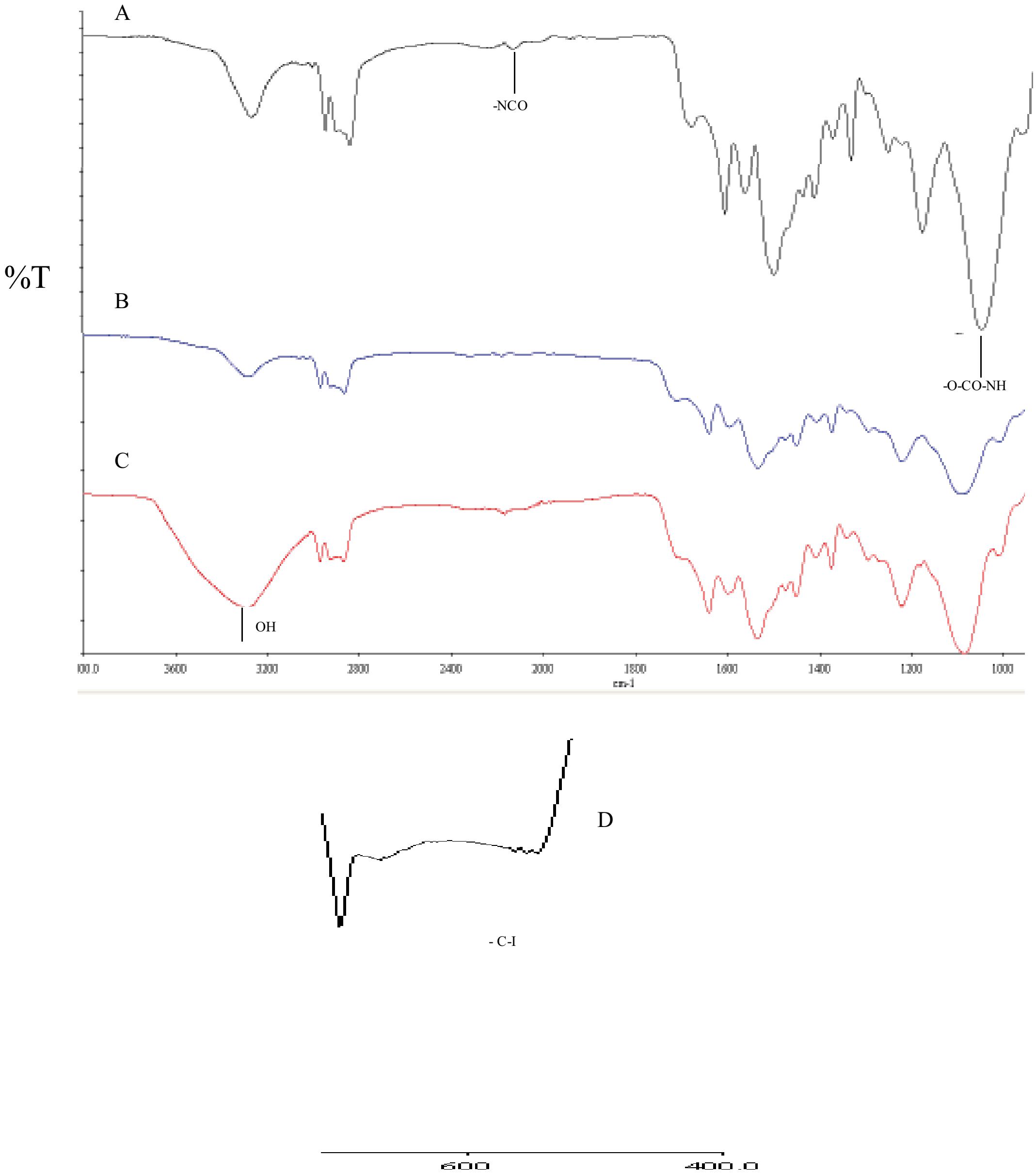

Fig. 2. Fourier-transform infrared spectra of PUF (A), I-PUF (B,D) and I-PUF-RhB (C).

molecules in solution. The pH_{pzc} of I-PUF value has been reported and determined from the plot of the initial pH vs. final pH is worth 3.5 [40]. At pH < pH_{pzc} = 3.5, the surface of the adsorbent is positively charged. At this pH, the adsorption of RhB is low due to competition between H^+ ions and RhB molecules to occupy the uptake sites that lead to electrostatic repulsion between the adsorbent surface and the RhB cations. Moreover, at pH > 3.7 (pKa = 3.7), the zwitterionic form dominants at pH greater than RhB pKa due to the electrostatic attraction that occurs between the xanthene and the carboxyl groups of RhB monomers, resulting in the formation of a larger molecular form (dimer). Besides, at pH > pH_{pzc} = 3.5, the surface of the adsorbent is negatively charged, leading to repulsing with the predominant species of RhB (the zwitterionic form and the dimer of the dye). Thus, the zwitterionic and dimer forms of RhB are accumulated, leading to the inability to enter the pores and, subsequently, a decrease in RhB adsorption [44–46]. Researchers previously reported that the optimum adsorption of RhB has occurred at pH ≈ 3 [44,46]. Subsequent retention profile experiments were taken at the optimum pH ≈ 3 ± 0.2.

3.2.2. *Effect of dose of I-PUF on the adsorption of RhB dye*

The adsorbent dose is one of the critical and efficacious parameters affecting the optimization of extraction percentage and the adsorption capacity. The effect of the I-PUF dose on the adsorption of RhB was investigated. The extraction percentage increased as the adsorbent dose increased from 0.05 to 0.1 g. The equilibrium in extraction percentage was observed after 0.1 g, as shown in Fig. 4B. The increase in extraction percentage from 0.05 to 0.1 g can be attributed

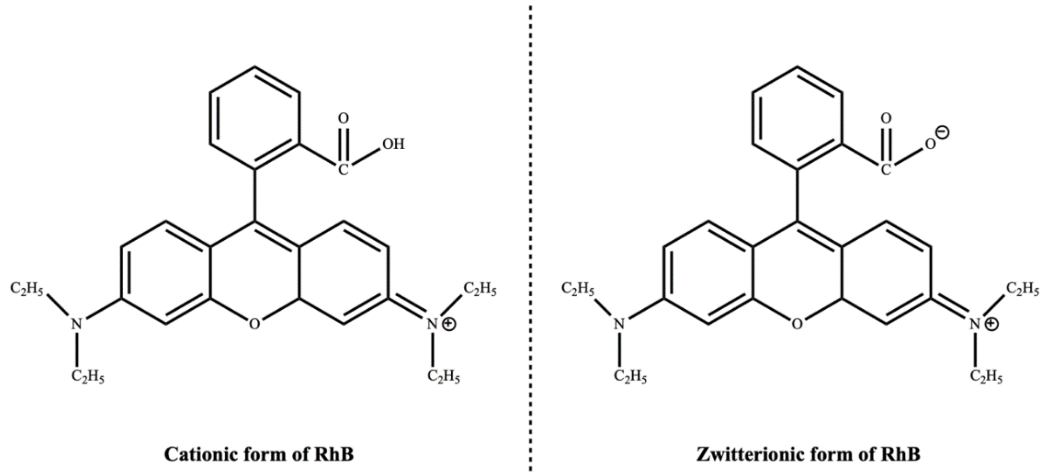

Fig. 3. Structure forms of RhB dye (A) cationic and (B) zwitterionic.

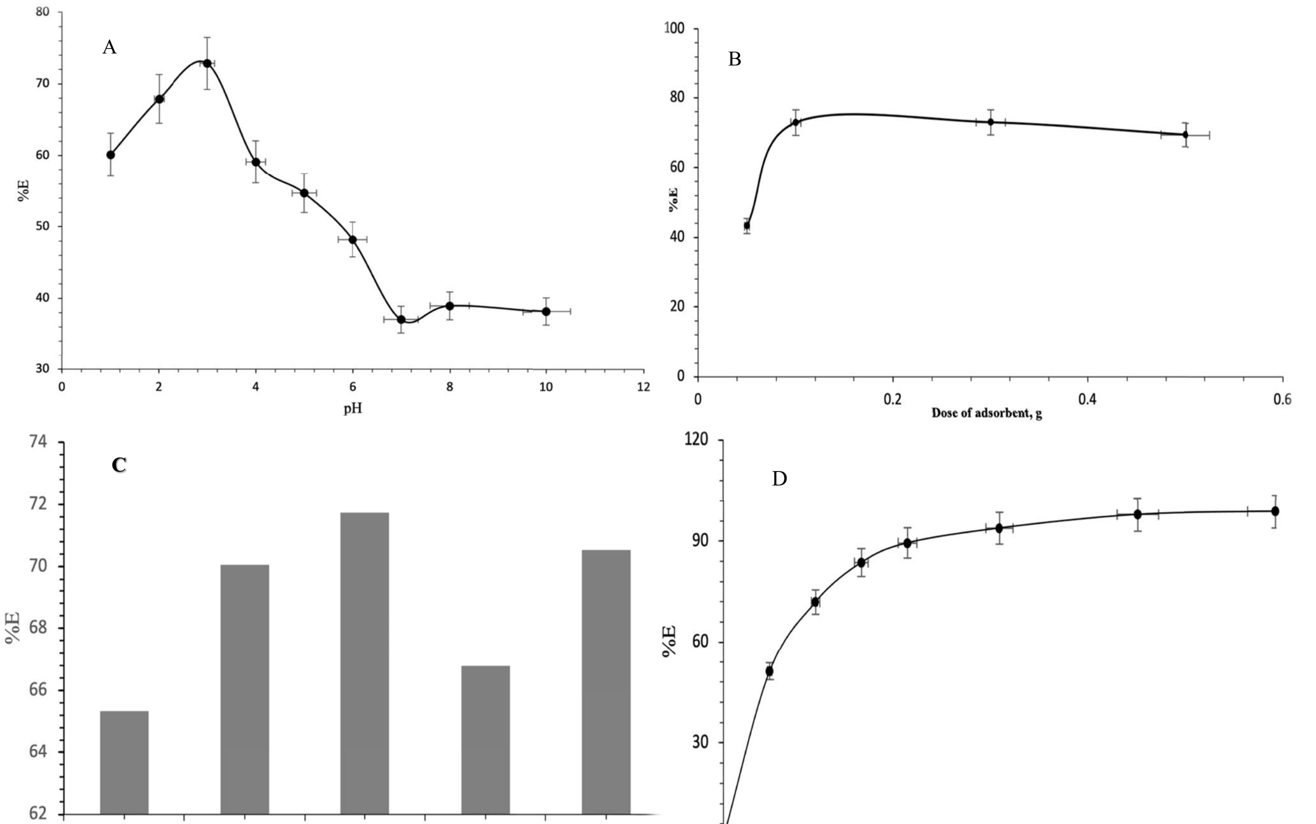

Fig. 4. Retention profile of Rhodamine B dye from aqueous solution onto I-PUF *via* a variety of effects pH (A), dose (B), mineral acid (C) and time (D) at (0.1 ± 0.002 g) after 30 min shaking time at 25°C ± 0.1°C.

to the increase in activation sites on the adsorbent surface. Besides, the slight decrease in extraction percentage after 0.1 g can be explained by agglomerations of particles onto the adsorption sites, leading to a decrease in adsorption surface area and extraction percentage [45,47].

3.2.3. *Effect of mineral acid and acidity on the adsorption of RhB dye onto I-PUF*

The influence of the mineral acids (HCl, HNO_3, H_2SO_4, $HClO_4$ and H_3PO_4) at 0.5 mol·L^{-1} on RhB adsorption onto the I-PUF sorbent was investigated. The results indicate that the maximum adsorption of RhB was achieved in the presence of HNO_3 as a suitable extraction medium (Fig. 4C). Accordingly, the effect of acidity on RhB adsorption by the used solid extractor was investigated using known concentrations in the range of 0.02–2 mol·L^{-1} of HNO_3. The results demonstrated that the maximum extraction of RhB was achieved at 0.5 mol·L^{-1} of HNO_3. Thus, 0.5 mol·L^{-1} of HNO_3 was selected for adjusting the acidity in the subsequent work.

3.2.4. Effect of shaking time on the adsorption of RhB dye

The effect of shaking time (0.0–60 min) on the adsorption of RhB from the aqueous solution under the optimized parameters was also investigated. The results obtained are demonstrated in Fig. 4D. In the beginning, the extraction of RhB was fast, and more than 80% was achieved in 20 min. After that, the maximum equilibrium value reached 30 min and stabilized over time. When the equilibrium time is short, the surface area is high. Therefore, the high adsorption in the primary time can be attributed to unoccupied active sites and the high dye concentration. On the other hand, the adsorption of RhB becomes slow at equilibrium due to the saturation of the surface with RhB molecules [48]. Thus, the subsequent work adopted a shaking time of 30 min.

3.3. Kinetic behavior of RhB adsorption onto I-PUF

The study of adsorption kinetics is significant as it predicts the reaction pathways and the mechanism of adsorption reactions. The potential dye adsorption mechanism, as well as the possible rate of controlling steps, can be investigated through non-linear kinetics models (Lagergren's pseudo-first-order, pseudo-second-order, Avrami and Elovich) and kinetic models of intraparticle diffusion (Weber–Morris, Reichenberg and Bangham) [8].

3.3.1. Pseudo-first-order model

The pseudo-first-order equation is the earliest model for explaining the adsorption rate in a solid solution. Lagergren suggested it in 1898 for oxalic and malonic acid adsorption on charcoal. This model is based on the adsorbent capacity and can be expressed by the study of Lima et al. [49]:

$$q_t = q_e \times \left[1 - \exp\left(-k_1 \times t\right)\right] \quad (1)$$

where q_e and q_t represent the amount of RhB adsorbed onto I-PUF at equilibrium and at a time (mg·g^{-1}), respectively. k_1 (min^{-1}) is the adsorption constant rate of Lagergren's first order. t is time (min). The correlation coefficient R^2 value for RhB adsorption onto I-PUF was calculated as 0.9998, as shown in Fig. 5A. The constant rate of Lagergren's first order k_1 was found to equal 0.231 min^{-1}. The q_e amounted to 2.403.

3.3.2. Pseudo-second-order model

The pseudo-second-order was initially used to describe the adsorption of divalent peat by Ho et al. [50]. It supposes that the adsorption occurs at two active adsorption sites [51]. The experimental data were subjected to study by pseudo-second-order. This model can be expressed by the study of Lima et al. [49]:

$$q_t = \frac{q_e^2 \times k_2 \times t}{\left[1 + \left(k_2 \times q_e \times t\right)\right]} \quad (2)$$

where q_e and q_t represent the amount of RhB adsorbed onto I-PUF at equilibrium and time (mg·g^{-1}), respectively. k_2 is the adsorption constant rate of the pseudo-second-order (min^{-1}). The k_2 was equal to 0.155. The correlation coefficient R^2 was obtained from Fig. 5B. The q_e was found 2.602 mg·g^{-1}.

The results showed that the adsorption process of RhB onto I-PUF obeys the pseudo-second-order kinetic instead of the pseudo-first-order kinetic for the following reasons. Firstly, the correlation coefficient R^2 of the pseudo-second-order kinetic model 0.9999 was slightly higher than the pseudo-first-order kinetic model 0.9998. Secondly, the experimental adsorption capacity (2.50 mg·g^{-1}) was closer to the calculated adsorption capacity of the pseudo-second-order kinetic model (2.602 mg·g^{-1}), whereas the adsorption capacity of the pseudo-first-order kinetic model calculated (2.403 mg·g^{-1}) was not consistent with the experimental data. These results indicate that the absorption process is controlled by chemisorption. Moreover, from the characteristic of chemical adsorption processes, only the active sites on the surface attracted the molecules, not all points on the surface to form a single layer [52]. Also, Liu [53] proposed that the pseudo-second-order model related to the existence of the active adsorption sites on the adsorbent's surface instead of the solution concentration (adsorbate). Similar trends have been reported for the adsorption of RhB dye from aqueous solutions by other adsorbents following the pseudo-second-order model [54–56].

3.3.3. Elovich model

Elovich model was developed by Zeldowitsch in 1934 and is generally known as Elovich model. It was first used to characterize the carbon monoxide and manganese dioxide adsorption rate. Elovich model is commonly used for systems in which the adsorbing surface is heterogeneous and for chemisorption processes [57–59]. Elovich model equation in Eq. (3) [60]:

$$q_e = \frac{1}{\beta}\ln\left(1 + \alpha\beta t\right) \quad (3)$$

where β (g·mg^{-1}) is the desorption coefficient related to the surface coverage extent and the activation energy for chemisorption. α (mg·g^{-1}·min^{-1}) is the Elovich constant related to the initial rate of RhB dye adsorption onto the adsorbent. The parameters were calculated from Fig. 5C. The results showed that α and β were 30.482 mg·g^{-1}·min^{-1} and 3.392 mg·g^{-1}, respectively. The correlation factor R^2 was found to be equal to 0.9999. α is a constant related to the rate of chemisorption and is usually higher than β. In other words, the absorption rate is higher than desorption. Thus, it can be indicated that the I-PUF surface is heterogeneous, the adsorption process is chemisorption, and the I-PUF has active sites for the rapid absorption of RhB molecules with a significant tendency to the adsorption [61].

3.3.4. Avrami model

Avrami model is one of the models that describe kinetic behaviour. It suggests that the reaction is located on the active surface sites of the sorbent [8,62]. The linearized Avrami model can be represented in Eq. (4) [63].

$$q_t = q_e\left(1-\exp\left(k_{av}t\right)^{n_{av}}\right) \quad (4)$$

where k_{av} (min^{-1}) is the Avrami kinetic constant rate, n_{av} is the constant related to the adsorption. q_e, q_t and t have their usual meanings. Avrami model parameters n_{av} and k_{av} were obtained from Fig. 5D. The value of k_{av} and n_{av} were equal to 0.093 and 0.357, respectively. The correlation factor R^2 is 1.

The constant n is considered the most significant factor in the Avrami model. Accordingly, its value plays a vital role in changes in the adsorption mechanism. Several authors suppose that the n factor affords a general idea about the reaction mechanism and determines the region where these adsorption reactions occur. Therefore, if $n_{av} > 1$, the adsorption is limited by surface reactions, and the diffusion of molecules is faster. While if n_{av} £ 1, the probability of the adsorption occurring is the same in any adsorbent region and is called homogenous adsorption [64,65]. The value of n_{av} was less than 1, indicating a significant homogeneity in adsorption between the adsorbent and adsorbate [64]. The parameter values of kinetics models are summarized in Table 1.

Table 1
Kinetic parameters for RhB adsorption onto I-PUF at 25°C ± 1°C

Kinetic models	Parameters	Values	R^2
Pseudo-first-order	$q_{e,\exp}$ (mg·g^{-1})	2.500	0.9998
	$q_{e,\text{cal}}$ (mg·g^{-1})	2.403	
	k_1 (min^{-1})	0.231	
Pseudo-second-order	$q_{e,\exp}$ (mg·g^{-1})	2.481	0.9999
	$q_{e,\text{cal}}$ (mg·g^{-1})	2.602	
	k_2 (g·mg^{-1}·min^{-1})	0.155	
Elovich	α (mg·g^{-1}·min^{-1})	30.483	0.9999
	β (mg·g^{-1})	3.393	
Avrami	k_{av}	0.093	1
	n_{av}	0.357	

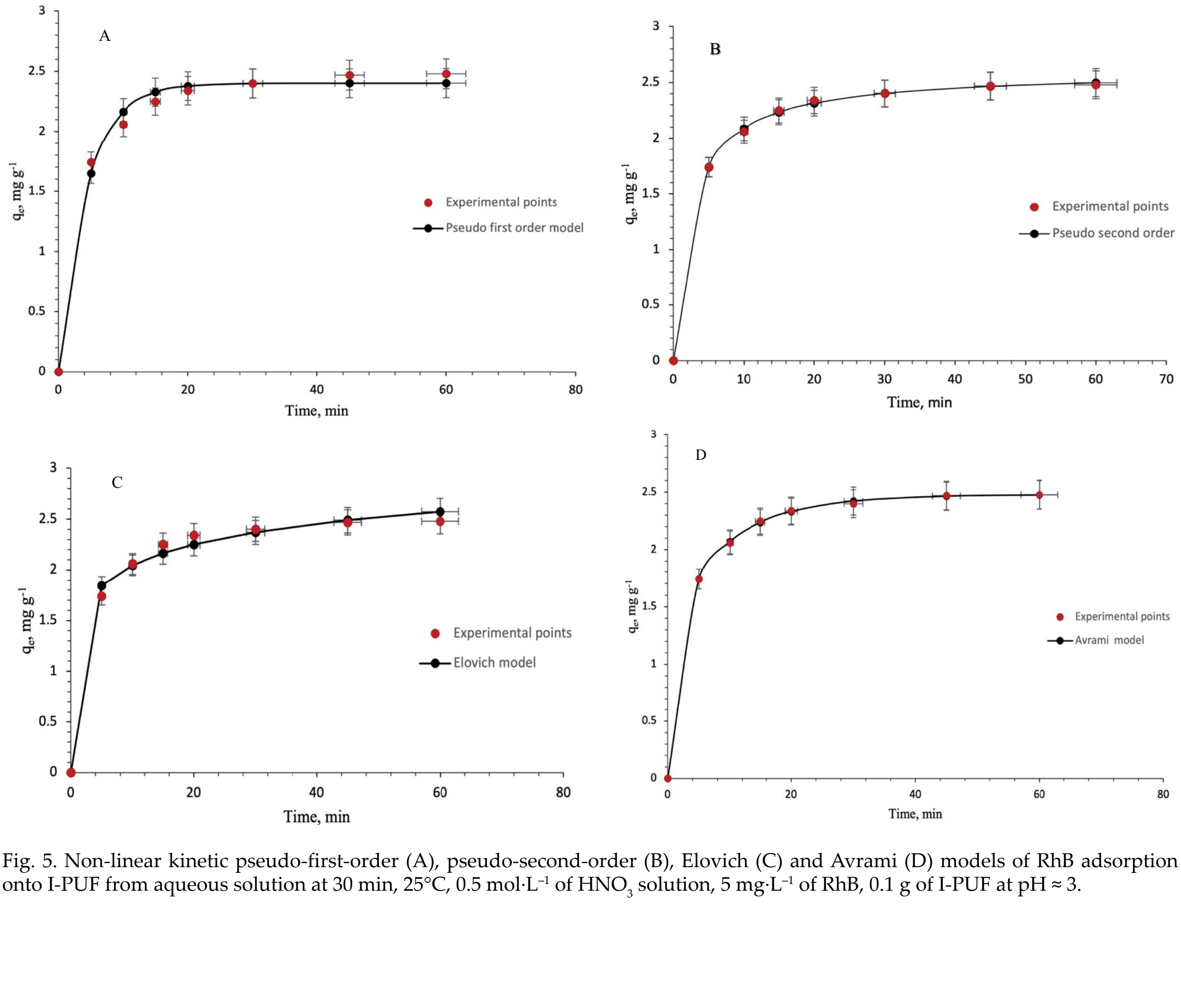

Fig. 5. Non-linear kinetic pseudo-first-order (A), pseudo-second-order (B), Elovich (C) and Avrami (D) models of RhB adsorption onto I-PUF from aqueous solution at 30 min, 25°C, 0.5 mol·L^{-1} of HNO_3 solution, 5 mg·L^{-1} of RhB, 0.1 g of I-PUF at pH ≈ 3.

3.4. Intraparticle diffusion kinetic models of RhB adsorption onto I-PUF

Understanding and explaining the adsorption system, dynamic behaviour and determination of the rate-limiting-step are considered pivotal steps in controlling the treatment processes and optimizing the design of adsorbents and adsorption conditions. Generally, molecules are adsorbed on an adsorbent through several steps. Firstly, in film diffusion, the RhB dye molecules are carried to the external surface of I-PUF. Secondly, in intraparticle diffusion, the dye molecules are adsorbed inside the pores of the I-PUF adsorbent. Thirdly, RhB molecules are adsorbed to the internal I-PUF surface, and this step often was not referred to as a rate-limiting step due to its fast occurrence. The Weber–Morris, Reichenberg and Bangham models are commonly used to study the absorption mechanism.

3.4.1. Weber–Morris model

The intraparticle diffusion kinetic model, or what is known as the Weber–Morris model, was applied to determine the intraparticle diffusion parameters of RhB adsorption onto I-PUF. This model is widely utilized for characterizing the adsorption mechanism, especially for porous sorbents such as PUF [66]. The model can be represented in Eq. (5) [67]:

$$q_t = R_d t^{1/2} + C \quad (5)$$

where q_t (mg·g⁻¹) is the adsorbed analyte concentration at time t. R_d (mg·g⁻¹·min⁻¹/²) is the rate constant of intraparticle diffusion. C (mg·g⁻¹) is the thickness of the boundary layer. The calculated values of R_d from the two slopes in the initial and second stages of the linear plots were found to be 0.3323 and 0.0585 mg·g⁻¹·min⁻¹/², respectively. R^2 was 0.9980 and 0.9100, respectively, as shown in Fig. 6A. Relative to the intercept C_1 and C_2 values, they amounted to 0.9862 and 2.055, respectively.

For the Weber–Morris model, if intraparticle diffusion is the only rate-limiting step, the q_t vs. $t^{-1/2}$ plot must pass through the origin [68]. Thus, from Fig. 6A the plot does not give a linear straight segment and does not cross the origin C¹0. It can be concluded that intraparticle diffusion is involved in adsorption but is not the only mechanism limiting adsorption kinetics. As a result, the adsorption mechanism is controlled by both film diffusion and intraparticle diffusion simultaneously [69,70].

Multilinearity indicates that the adsorption process is controlled by multiple mechanisms, where each linear segment represents a specific controlling mechanism. Fig. 6A shows that the plot is not linear through the adsorption time and can be separated into two linear regions. The first line represents surface adsorption as the beginning of the process, meaning that the RhB molecules were transferred to the outer surface of the I-PUF through film diffusion. The second line represents the intraparticle diffusion as the end of the process, which means that the RhB molecules are diffused inside I-PUF pores by intraparticle diffusion [48,69]. In other words, the plot of q_t vs. $t^{-1/2}$ was a straight line until 15 min. After that, the plot deviated with increasing time, indicating that the diffusion rate was high at the initial stage due to all the adsorbent's unoccupied active sites. In the second step, intraparticle diffusion increased slightly with the depletion of adsorbent pores. Thus, RhB adsorption was fast, then decreased over time because of the preoccupation of the active positions on the adsorbing surface (>15 min) [71].

The intercept C value provides information about the boundary layer thickness. The boundary layer effect is paramount when the intercept is considerable. Increasing the C values from one stage to another indicates the boundary layer effect [72]. Moreover, the particle pore dimensions contribute to controlling intraparticle diffusion. The larger the particle size pores, the lower the intraparticle diffusion resistance to control the adsorption kinetics for high-porous

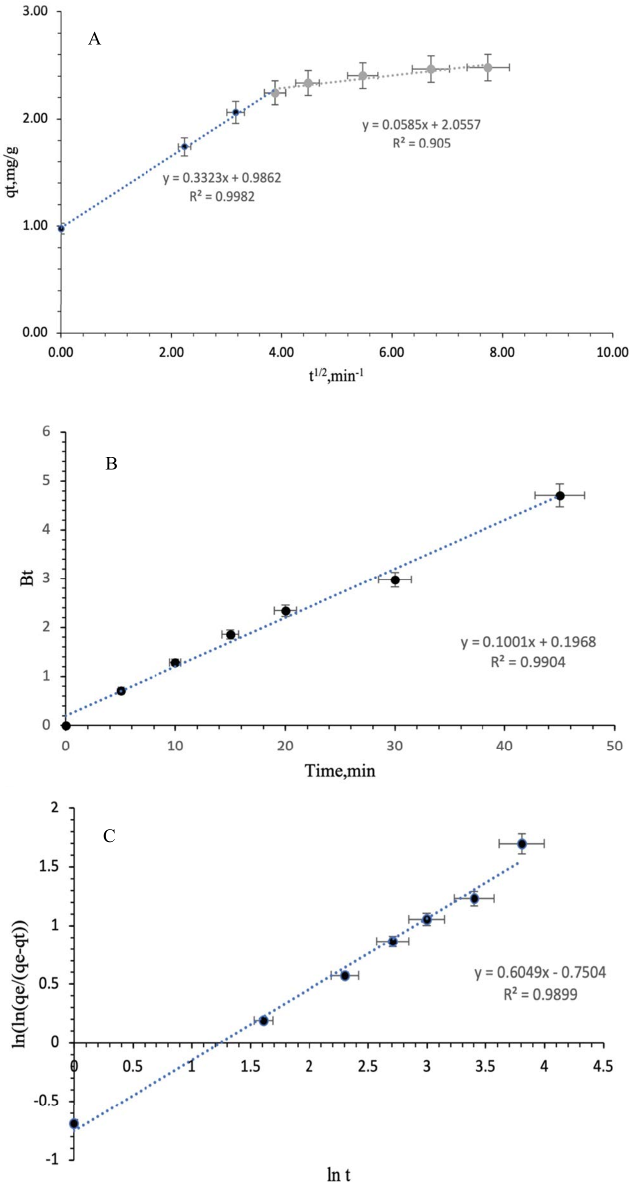

Fig. 6. Intraparticle diffusion kinetic models of RhB adsorption onto I-PUF Weber–Morris (A), Reichenberg (B) and Bangham (C) from aqueous solution at 30 min, 25°C, 0.5 mol·L⁻¹ of HNO_3 solution, 5 mg·L⁻¹ of RhB, 0.1 g of I-PUF at pH ≈ 3.

materials decreases. In other words, it decreases the effect of the boundary layer [73].

3.4.2. Reichenberg model

Reichenberg's model is called the Boyd model or Boyd's intraparticle diffusion model [74]. This model can be used to determine and distinguish whether interparticle diffusion or film diffusion mechanisms it is controlling the adsorption rate. Therefore, the contribution of the pore diffusion mechanism in RhB adsorption onto I-PUF was tested. Reichenberg model [75] expressed in Eq. (6) was applied.

$$B_t = -0.4977 - \ln\left(1 - F\right) \quad (6)$$

where B_t is Reichenberg constant. q_t is the value of RhB molecules adsorbed into the I-PUF at time t (mg·g^{-1}). q_e is the value of RhB molecules adsorbed into the I-PUF at equilibrium (mg·g^{-1}). The B_t value is a mathematical function of F that can be calculated from the mathematical relationship in Eq. (7):

$$F = \frac{q_t}{q_e} \quad (7)$$

The plot of B_t vs. ln(1 – q_t/q_e) results in a straight line, in which the correlation factor R^2 value amounted to 0.9904, as shown in Fig. 6B. The straight line does not pass through the origin, indicating that the film diffusion controls the absorption rate besides intraparticle diffusion. If the straight line passes through the origin, the absorption rate is controlled by intraparticle diffusion [8,76].

3.4.3. Bangham model

Bangham model determines whether the pore diffusion mechanism controls the adsorption of RhB onto the I-PUF. The Bangham model [77] is expressed in Eq. (8):

$$\ln\left(\ln\left(\frac{q_e}{\left(q_e - q_t\right)}\right)\right) = \ln k_B + \alpha \ln t \quad (8)$$

where q_e, q_t and t have their usual meanings. k_B is Bangham's constant. The Bangham model in Fig. 6C resulted in a linear curve. The correlation coefficient R^2 obtained from the plot of ln(ln($q_e/q_e - q_t$)) vs. ln$t$ is equal to 0.9899. The k_B 1.8310 and α 0.7504 were calculated from the intercept and slope, respectively, as shown in Fig. 6C. The linear plot of the Bangham model does not pass through the origin, suggesting that pore diffusion was involved in the adsorption of RhB onto I-PUF but not the only rate-controlling step [78]. Overall, the results of intraparticle diffusion kinetic models assumed that the adsorption mechanism of RhB onto I-PUF may be controlled by film diffusion, intraparticle diffusion and pore diffusion. The parameters of Weber–Morris, Reichenberg and Bangham models are summarized in Table 2.

Table 2
Intraparticle diffusion parameters for RhB adsorption onto I-PUF at 25°C ± 1°C

Intraparticle diffusion models	Parameters	Values	R^2
Weber–Morris	R_{d1} (mg·g^{-1}·min$^{-1/2}$)	0.3323	0.9980
	R_{d2} (mg·g^{-1}·min$^{-1/2}$)	0.0585	
	C_1	0.9862	0.9100
	C_2	2.0557	
Bangham	α	0.7504	0.9899
	k_B	1.8310	
Reichenberg	–	–	0.9904

3.5. Adsorption isotherm models of RhB adsorption onto I-PUF

The adsorption isotherm is generally described as the transmission of pollutants from an aqueous phase to a solid phase at a constant pH and temperature. Moreover, it provides information about the adsorption capacity and the interaction mechanism between the adsorbate and the adsorbent [69].

3.5.1. Langmuir isotherm model

Langmuir's adsorption isotherm model describes the homogeneous adsorption reactions where this model assumes that the adsorption occurs on one activation site and that each molecule has constant enthalpy and activation energy to form an adsorption monolayer. The non-linearized form of the Langmuir model can be expressed in Eq. (9) [79]:

$$q_e = \frac{q_m K_l C_e}{\left(1 + K_l C_e\right)} \quad (9)$$

where q_m (mg·g^{-1}) is the maximum adsorption capacity needed for the surface monolayer coverage. K_L (L·mg^{-1}) is the Langmuir constant. q_e (mg·g^{-1}) is the adsorption capacity. C_e (mg·L^{-1}) is the equilibrium concentration.

From Fig. 7A, the q_m and K_L were equal to 22.032 mg·g^{-1} and 1.105 L·mg^{-1}, respectively. The correlation coefficient R^2 was 0.9963. The adsorption favorability toward dye can be described by calculating the separation factor R_L [79]:

$$R_L = \frac{1}{1 + K_L C_e} \quad (10)$$

where K_L (L·mg^{-1}) and C_e (mg·L^{-1}) represent the Langmuir constant and the initial RhB concentration, respectively. R_L value refers to the adsorption nature. When $R_L > 1$, the adsorption is unfavourable. $R_L = 1$, the adsorption is linear, and the adsorption is favourable when $0 < R_L < 1$. The adsorption is irreversible when $R_L = 0$. The R_L values were (0.2–0.7), which indicates that the adsorption of RhB onto I-PUF was favourable at 25°C and various initial concentrations of RhB.

3.5.2. Freundlich isotherm model

The Freundlich isotherm model describes adsorption occurring on multilayers with unequal heat and affinities

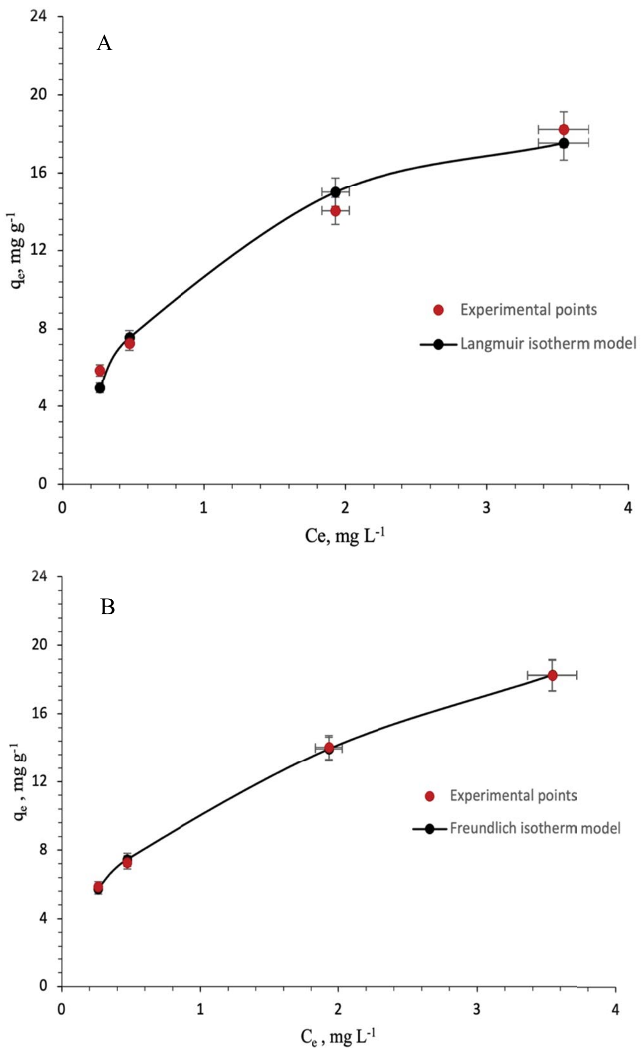

Fig. 7. Non-linear isotherm models of RhB adsorption onto I-PUF Langmuir (A) and Freundlich (B) from aqueous solution at 30 min, 25°C, 0.5 mol·L⁻¹ of HNO_3 solution, 5 mg·L⁻¹ of RhB, 0.1 g of I-PUF at pH ≈ 3.

distribution on heterogeneous surfaces. The non-linearized form of the Freundlich model can be expressed in Eq. (11) [80]:

$$q_e = K_f C_e^{1/n} \quad (11)$$

where K_f is Freundlich's constant. n is the adsorption intensity or heterogeneity of the surface. From Fig. 7B, the K_f and $1/n$ were found to be equal to 10.412 mg·g⁻¹ and 2.250, respectively. The correlation coefficient R^2 was 0.9999. $1/n$ value refers to the adsorption nature. When $1/n < 1$ or $1/n > 1$, the adsorption is favourable and unfavourable, respectively. When $1/n = 1$, the Freundlich model is linear, and the adsorbent surface is heterogeneous when $0 < 1/n < 1$ [80]. The $1/n$ values were 0.445, which indicates that the adsorption of RhB onto I-PUF was favourable at 25°C and occurred on a heterogeneous adsorbent surface. The maximum adsorption capacity of RhB onto I-PUF and the contact time were compared with other adsorbents and are summarized in Table 3.

Table 3
Maximum adsorption capacity of I-PUF and the contact time compared to other adsorbents

Adsorbent	q_m (mg·g⁻¹)	Time (min)	References
Modified zeolite	7.955	200	[81]
Walnut shell	2.292	40	[82]
Activated carbon	5.338	30	[83]
Rice husk	5.873	180	[83]
Iodo-polyurethane foam	22.032	30	This study

3.6. Thermodynamic parameters of RhB adsorption onto I-PUF

Thermodynamic adsorption is a significant factor in predicting the types and mechanisms of the adsorption process under different temperatures and optimum conditions, such as pH, the dose of adsorbent, and the solution acidity. Therefore, the temperature effect on the adsorption of RhB onto I-PUF was studied by the calculation of the adsorption enthalpy change ($\Delta H°$), entropy change ($\Delta S°$), and the Gibbs free energy change ($\Delta G°$) *via* van't Hoff equations [84]:

$$K_d = \frac{q_e}{C_e} \quad (12)$$

$$\ln K = \frac{\Delta S°}{R} - \frac{\Delta H°}{RT} \quad (13)$$

$$\Delta G° = -RT \ln K_d \quad (14)$$

$$\Delta G° = \Delta H° - T\Delta S° \quad (15)$$

where K_d is the distribution coefficient for RhB adsorption, R is the gas constant (8.314 J·mol⁻¹·K⁻¹). T is the temperature in Kelvin. Fig. 8 shows a linear relationship between $\ln K_d$ vs. $1/T$ for the adsorption of RhB onto I-PUF (R^2 = 0.9942). The values of $\Delta H°$ and $\Delta S°$ can be calculated from the slope and intercept, respectively. The Gibbs energy values contribute to the determination of the spontaneity interaction. The average negative $\Delta G°$ values (–19.4655 kJ·mol⁻¹) indicated spontaneous adsorption behaviour. Meanwhile, the $\Delta H°$ for the adsorption of RhB onto I-PUF was negative value (–31.4884 kJ·mol⁻¹), meaning that the adsorption process is exothermic chemisorption [33]. The decrease in adsorption capacity is most often associated with the temperature increase in exothermic reactions. The exothermic term denotes that the total energy absorbed in bond breaking is less than the total energy emitted in the bond formation between RhB molecules and I-PUF, which releases excess energy in a heat form [85].

Overall, if the resulting $\Delta H°$ value is lower than 20.90 kJ·mol⁻¹, the intermolecular bonding type is Van der Waals' bonding, and the adsorption is known as physical adsorption. In the case of the resulting $\Delta H°$ values in the range (20.90–418.4 kJ·mol⁻¹), the intermolecular bonding type is chemical bonding, and the adsorption is known as chemical adsorption [86]. The $\Delta H°$ value was obtained at –31.4884 kJ·mol⁻¹, demonstrating that chemical adsorption is dominant between RhB molecules and I-PUF.

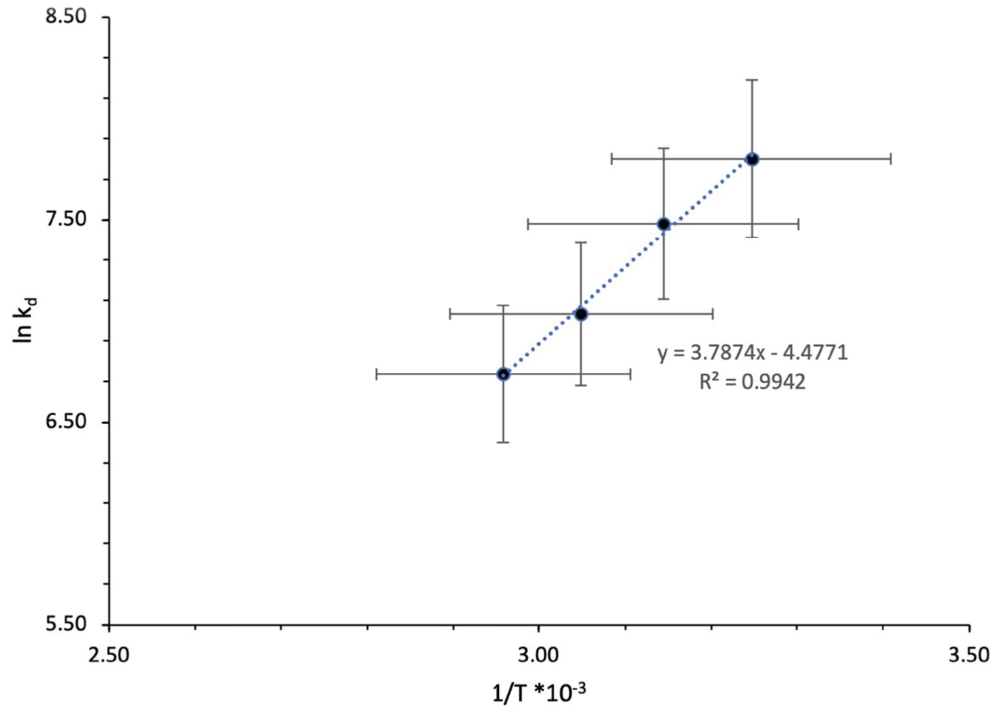

Fig. 8. Van't Hoff plot for RhB adsorption from aqueous solution at 30 min, 25°C, 0.5 mol·L^{-1} of HNO_3 solution, 5 mg·L^{-1} of RhB, 0.1 g of I-PUF at pH ≈ 3.

In contrast, the values of $\Delta S°$ were negative (−37.2226 kJ·mol^{-1}). The negative value of $\Delta S°$ demonstrates that no effective modification occurred in the internal structures of the I-PUF during the adsorption process. In addition, it suggests a decrease in the degrees of randomness (low disorder) at the solid/solution interface during RhB adsorption onto I-PUF [33,87].

4. Conclusion

The present study has demonstrated that the I-PUF was an efficient and suitable adsorbent for the adsorption of RhB successfully from aqueous media. The maximum adsorption of RhB was achieved at pH ≈ 3. The results of kinetic models indicated that the adsorption of RhB obeyed the pseudo-second-order and Freundlich model. The adsorption process was controlled through chemisorption. The intraparticle diffusion models indicated that the adsorption of RhB onto I-PUF was controlled by film diffusion, intraparticle diffusion and pore diffusion. The thermodynamic parameters (ΔH, ΔS and ΔG) indicated the exothermic and spontaneous nature of RhB adsorption by the I-PUF.

References

[1] H.M. Al-Saidi, A.A. El-Bindary, A.Z. El-Sonbati, M.A. Abdel-Fadeel, Fluorescence enhancement of Rhodamine B as a tool for the determination of trace and ultra-trace concentrations of bismuth using dispersive liquid–liquid microextraction, RSC Adv., 6 (2016) 21210–21218.

[2] T.O. Ajiboye, O.A. Oyewo, D.C. Onwudiwe, Adsorption and photocatalytic removal of Rhodamine B from wastewater using carbon-based materials, FlatChem, 29 (2021) 100277, doi: 10.1016/j.flatc.2021.100277.

[3] V. Kumar, P. Saharan, A.K. Sharma, A. Umar, I. Kaushal, A. Mittal, Y. Al-Hadeethi, B. Rashad, Silver doped manganese oxide-carbon nanotube nanocomposite for enhanced dye-sequestration: isotherm studies and RSM modelling approach, Ceram. Int., 46 (2020) 10309–10319.

[4] S. Shehu Imam, H. Funmilayo Babamale, A short review on the removal of Rhodamine B dye using agricultural waste-based adsorbents, Asian J. Chem. Sci., 7 (2020) 25–37.

[5] M. Tariq, M. Muhammad, J. Khan, A. Raziq, M.K. Uddin, A. Niaz, S.S. Ahmed, A. Rahim, Removal of Rhodamine B dye from aqueous solutions using photo-Fenton processes and novel Ni-Cu@MWCNTs photocatalyst, J. Mol. Liq., 312 (2020) 113399, doi: 10.1016/j.molliq.2020.113399.

[6] C. Arora, P. Kumar, S. Soni, J. Mittal, A. Mittal, B. Singh, Efficient removal of malachite green dye from aqueous solution using *Curcuma caesia* based activated carbon, Desal. Water Treat., 195 (2020) 341–352.

[7] L.B.L. Lim, N. Priyantha, X.Y. Fang, N.A.H. Mohamad Zaidi, *Artocarpusodoratissimus* peel as a potential adsorbent in environmental remediation to remove toxic Rhodamine B dye, J. Mater. Environ. Sci., 8 (2017) 494–502.

[8] M. Benjelloun, Y. Miyah, G.A. Evrendilek, F. Zerrouq, S. Lairini, Recent advances in adsorption kinetic models: their application to dye types, Arabian J. Chem., 14 (2021) 103031, doi: 10.1016/j.arabjc.2021.103031.

[9] N. Bhadusha, T. Ananthabaskaran, Kinetic, thermodynamic and equilibrium studies on uptake of Rhodamine B onto $ZnCl_2$ activated low-cost carbon, E-J. Chem., 9 (2012) 873026, doi: 10.1155/2012/873026.

[10] Toronto Research Chemicals, Identification of the Substance/Mixture and of the Company/Undertaking, Toronto, 2019.

[11] M.R.R. Kooh, L.B.L. Lim, L.H. Lim, M. Khairud Dahri, Separation of toxic Rhodamine B from aqueous solution using an efficient low-cost material, *Azolla pinnata*, by adsorption method, Environ. Monit. Assess., 188 (2016) 108, doi: 10.1007/s10661-016-5108-7.

[12] L.M. Skjolding, L.vG. Jørgensen, K.S. Dyhr, C.J. Köppl, U.S. McKnight, P. Bauer-Gottwein, P. Mayer, P.L. Bjerg, A. Baun, Assessing the aquatic toxicity and environmental safety of

tracer compounds Rhodamine B and Rhodamine WT, Water Res., 197 (2021) 117109, doi: 10.1016/j.watres.2021.117109.

[13] Y. Chao, J. Pang, Y. Bai, P. Wu, J. Luo, J. He, Y. Jin, X. Li, J. Xiong, H. Li, W. Zhu, Graphene-like BN@SiO_2 nanocomposites as efficient sorbents for solid-phase extraction of Rhodamine B and Rhodamine 6G from food samples, Food Chem., 320 (2020) 126666, doi: 10.1016/j.foodchem.2020.126666.

[14] Q. Liu, Q. Xu, W. Sun, Facile preparation of core-shell magnetic organic covalent framework via self-polymerization of two-in-one strategy as a magnetic solid-phase extraction adsorbent for determination of Rhodamine B in food samples, J. Chromatogr. A, 1657 (2021) 462566, doi: 10.1016/j.chroma.2021.462566.

[15] A. Mittal, R. Jain, J. Mittal, S. Varshney, S. Sikarwar, Removal of Yellow ME 7 GL from industrial effluent using electrochemical and adsorption techniques, Int. J. Environ. Pollut., 43 (2010) 308–323.

[16] Official Journal of the European Union, Commission Regulation (EU) No. 1129/2011 of 11 November 2011 Amending Annex II to Regulation (EC) No 1333/2008 of the European Parliament and of the Council by Establishing a Union List of Food Additives, 2011.

[17] Official Journal of the European Union, Regulation (Ec) No 1223/2009 of the European Parliament and the Council of 30 November 2009 on Cosmetic Products, 2009.

[18] A. Tkaczyk, K. Mitrowska, A. Posyniak, Synthetic organic dyes as contaminants of the aquatic environment and their implications for ecosystems: a review, Sci. Total Environ., 717 (2020) 137222, doi: 10.1016/j.scitotenv.2020.137222.

[19] eCFR: 21 CFR Part 74 — Listing of Color Additives Subject to Certification. Available at: https://www.ecfr.gov/current/title-21/chapter-I/subchapter-A/part-74

[20] E. Yilmaz, M. Soylak, A novel and simple deep eutectic solvent based liquid phase microextraction method for Rhodamine B in cosmetic products and water samples prior to its spectrophotometric determination, Spectrochim. Acta, Part A, 202 (2018) 81–86.

[21] Y. Fang, D. Hariu, T. Yamamoto, S. Komarov, Acoustic cavitation assisted plasma for wastewater treatment: degradation of Rhodamine B in aqueous solution, Ultrason. Sonochem., 52 (2019) 318–325.

[22] X. Xiao, X.-L. Ma, Z.-Y. Liu, W.-W. Li, H. Yuan, X.-B. Ma, L.-X. Li, H.-Q. Yu, Degradation of Rhodamine B in a novel bio-photoelectric reductive system composed of *Shewanella oneidensis* MR-1 and Ag_3PO_4, Environ. Int., 126 (2019) 560–567.

[23] W. Xiao, X. Jiang, X. Liu, W. Zhou, Z.N. Garba, I. Lawan, L. Wang, Z. Yuan, Adsorption of organic dyes from wastewater by metal-doped porous carbon materials, J. Cleaner Prod., 284 (2021) 124773, doi: 10.1016/j.jclepro.2020.124773.

[24] R. Bushra, S. Mohamad, Y. Alias, Y. Jin, M. Ahmad, Current approaches and methodologies to explore the perceptive adsorption mechanism of dyes on low-cost agricultural waste: a review, Microporous Mesoporous Mater., 319 (2021) 111040, doi: 10.1016/j.micromeso.2021.111040.

[25] W. Xiao, Z.N. Garba, S. Sun, I. Lawan, L. Wang, M. Lin, Z. Yuan, Preparation and evaluation of an effective activated carbon from white sugar for the adsorption of Rhodamine B dye, J. Cleaner Prod., 253 (2020) 119989, doi: 10.1016/j.jclepro.2020.119989.

[26] Z.-L. Cheng, Y.-X. Li, Z. Liu, Novel adsorption materials based on graphene oxide/beta zeolite composite materials and their adsorption performance for Rhodamine B, J. Alloys Compd., 708 (2017) 255–263.

[27] X. Duan, R. Lv, Z. Kong, An anionic metal-organic framework for selective adsorption separation toward methylene blue and Rhodamine B, J. Inorg. General Chem., 646 (2020) 1408–1411.

[28] A.A. Oyekanmi, A. Ahmad, K. Hossain, M.I. Rafatullah, Adsorption of Rhodamine B dye from aqueous solution onto acid treated banana peel: response surface methodology, kinetics and isotherm studies, PLoS One, 14 (2019) e0216878, doi: 10.1371/journal.pone.0216878.

[29] X. Wei, D. Chen, L. Wang, Y. Ma, W. Yang, Carboxylate-functionalized hollow polymer particles modified polyurethane foam for facile and selective removal of cationic dye, Appl. Surf. Sci., 579 (2022) 152153, doi: 10.1016/j.apsusc.2021.152153.

[30] B. Wang, Q. Zhang, G. Xiong, F. Ding, Y. He, B. Ren, L. You, X. Fan, C. Hardacre, Y. Sun, Bakelite-type anionic microporous organic polymers with high capacity for selective adsorption of cationic dyes from water, Chem. Eng. J., 366 (2019) 404–414.

[31] H. Zhao, X.-K. Ouyang, L.-Y. Yang, Adsorption of lead ions from aqueous solutions by porous cellulose nanofiber–sodium alginate hydrogel beads, J. Mol. Liq., 324 (2021) 115122, doi: 10.1016/j.molliq.2020.115122.

[32] T. Khan, V. Acar, M. Raci Aydin, B. Hülagü, H. Akbulut, M. Özgür Seydibeyoğlu, A review on recent advances in sandwich structures based on polyurethane foam cores, Polym. Compos., 41 (2020) 2355–2400.

[33] M. El Bouraie, A. Abdelghany, Sorption features of polyurethane foam functionalized with salicylate for chlorpyrifos: equilibrium, kinetic models and thermodynamic studies, Polymers (Basel), 12 (2020) 2036, doi: 10.3390/polym12092036.

[34] M. El-Bouraie, Removal of the malachite green (MG) dye from textile industrial wastewater using the polyurethane foam functionalized with salicylate, J. Dispersion Sci. Technol., 36 (2015) 1228–1236.

[35] S.T. Moghaddam, M.R. Naimi-Jamal, A. Rohlwing, F.B. Hussein, N. Abu-Zahra, High removal capacity of arsenic from drinking water using modified magnetic polyurethane foam nanocomposites, J. Polym. Environ., 27 (2019) 1497–1504.

[36] F. Wu, K. Pickett, A. Panchal, M. Liu, Y. Lvov, Superhydrophobic polyurethane foam coated with polysiloxane-modified clay nanotubes for efficient and recyclable oil absorption, ACS Appl. Mater. Interfaces, 11 (2019) 25445–25456.

[37] H. Qin, K. Wang, Study on preparation and performance of PEG-based polyurethane foams modified by the chitosan with different molecular weight, Int. J. Biol. Macromol., 140 (2019) 877–885.

[38] D. Yuan, T. Zhang, Q. Guo, F. Qiu, D. Yang, Z. Ou, A novel hierarchical hollow SiO_2@MnO_2 cubes reinforced elastic polyurethane foam for the highly efficient removal of oil from water, Chem. Eng. J., 327 (2017) 539–547.

[39] L. Ren, Z. Qiu, Z. Wang, D. Yang, D. Zhou, T. Zhang, Preparation of biomass carbon/polyurethane foams for selective oil/water absorption, J. Dispersion Sci. Technol., 41 (2020) 1872–1878.

[40] E.A. Moawed, M.A. El-Hagrasy, N.E.M. Embaby, Substitution influence of halo polyurethane foam on the removal of bismuth, cobalt, iron and molybdenum ions from environmental samples, J. Taiwan Inst. Chem. Eng., 70 (2017) 382–390.

[41] M.S. El-Shahawi, H. Alwael, A novel platform based on gold nanoparticles chemically impregnated polyurethane foam sorbent coupled ion chromatography for selective separation and trace determination of phosphate ions in water, Microchem. J., 149 (2019) 103987, doi: 10.1016/j.microc.2019.103987.

[42] M. Revenga-Parra, C. Gómez-Anquela, T. García-Mendiola, E. Gonzalez, F. Pariente, E. Lorenzo, Grafted Azure A modified electrodes as disposable β-nicotinamide adenine dinucleotide sensors, Anal. Chim. Acta, 747 (2012) 84–91.

[43] Z.M. Saigl, O.A. Aljuaid, Removal of Rhodamine dye from foodstuffs using column chromatography and isotherm study, Sep. Sci. Technol. (Philadelphia), 58 (2023) 1616–1629.

[44] A.A. Inyinbor, F.A. Adekola, G.A. Olatunji, Adsorption of Rhodamine B Dye from aqueous solution on *Irvingia gabonensis* biomass: kinetics and thermodynamics studies, S. Afr. J. Chem., 68 (2015) 115–125.

[45] A.A. Inyinbor, F.A. Adekola, G.A. Olatunji, Kinetics, isotherms and thermodynamic modeling of liquid phase adsorption of Rhodamine B dye onto *Raphia hookerie* fruit epicarp, Water Resour. Ind., 15 (2016) 14–27.

[46] M. Zamouche, O. Hamdaoui, Sorption of Rhodamine B by cedar cone: effect of pH and ionic strength, Energy Procedia, 18 (2012) 1228–1239.

[47] S.S.A. Alkurdi, R.A. Al-Juboori, J. Bundschuh, L. Bowtell, A. Marchuk, Inorganic arsenic species removal from water using bone char: a detailed study on adsorption kinetic and isotherm models using error functions analysis, J. Hazard. Mater., 405 (2021) 124112, doi: 10.1016/j.jhazmat.2020.124112.

[48] M. Ghaedi, Sh. Heidarpour, S.N. Kokhdan, R. Sahraie, A. Daneshfar, B. Brazesh, Comparison of silver and palladium nanoparticles loaded on activated carbon for efficient removal of methylene blue: kinetic and isotherm study of removal process, Powder Technol., 228 (2012) 18–25.
[49] E.C. Lima, F. Sher, A. Guleria, M.R. Saeb, I. Anastopoulos, H.N. Tran, A. Hosseini-Bandegharaei, Is one performing the treatment data of adsorption kinetics correctly?, J. Environ. Chem. Eng., 9 (2021) 104813, doi: 10.1016/j.jece.2020.104813.
[50] Y.S. Ho, D. Wase', C.F. Forster, Removal of lead ions from aqueous solution using sphagnum moss peat as adsorbent, Water SA, 22 (1996) 219–224.
[51] H.K. Boparai, M. Joseph, D.M. O'carroll, Kinetics and thermodynamics of cadmium ion removal by adsorption onto nano zerovalent iron particles, J. Hazard. Mater., 186 (2011) 458–465.
[52] M.M. Góes, M. Keller, V. Masiero Oliveira, L.D.G. Villalobos, J.C.G. Moraes, G.M. Carvalho, Polyurethane foams synthesized from cellulose-based wastes: kinetics studies of dye adsorption, Ind. Crops Prod., 85 (2016) 149–158.
[53] Y. Liu, New insights into pseudo-second-order kinetic equation for adsorption, Physicochem. Eng. Aspects, 320 (2008) 275–278.
[54] H.M. Al-Saidi, M.A. Abdel-Fadeel, S.S. Alharthi, Preconcentration and ultrasensitive spectrophotometric estimation of tungsten in soils using polyurethane foam in the presence of Rhodamine B: kinetic and thermodynamic studies, and designing a simple automated preconcentration system, J. Saudi Chem. Soc., 25 (2021) 101301, doi: 10.1016/j.jscs.2021.101301.
[55] U. Jinendra, D. Bilehal, B.M. Nagabhushana, A. Praveen Kumar, Adsorptive removal of Rhodamine B dye from aqueous solution by using graphene–based nickel nanocomposite, Heliyon, 7 (2021) e06851, doi: 10.1016/j.heliyon.2021.e06851.
[56] R. Ghibate, O. Senhaji, R. Taouil, Kinetic and thermodynamic approaches on Rhodamine B adsorption onto pomegranate peel, Case Stud. Chem. Environ. Eng., 3 (2021) 100078, doi: 10.1016/j.cscee.2020.100078.
[57] J. Wang, X. Guo, Adsorption kinetic models: physical meanings, applications, and solving methods, J. Hazard. Mater., 390 (2020) 122156, doi: 10.1016/j.jhazmat.2020.122156.
[58] M. Rajabi, K. Mahanpoor, O. Moradi, Preparation of PMMA/GO and PMMA/GO-Fe_3O_4 nanocomposites for malachite green dye adsorption: kinetic and thermodynamic studies, Composites, Part B, 167 (2019) 544–555.
[59] J.C.P. Vaghetti, E.C. Lima, B. Royer, B.M. da Cunha, N.F. Cardoso, J.L. Brasil, S.L.P. Dias, Pecan nutshell as biosorbent to remove Cu(II), Mn(II) and Pb(II) from aqueous solutions, J. Hazard. Mater., 162 (2009) 270–280.
[60] M.T. Amin, A.A. Alazba, M. Shafiq, Successful application of *Eucalyptus camdulensis* biochar in the batch adsorption of crystal violet and methylene blue dyes from aqueous solution, Sustainability (Switzerland), 13 (2021) 3600, doi: 10.3390/su13073600.
[61] Z.R. Lopičić, M.D. Stojanović, S.B. Marković, J.V. Milojković, M.L. Mihajlović, T.S. Kaluđerović Radoičić, M.L.j. Kijevčanin, Effects of different mechanical treatments on structural changes of lignocellulosic waste biomass and subsequent Cu(II) removal kinetics, Arabian J. Chem., 12 (2019) 4091–4103.
[62] K.L. Tan, B.H. Hameed, Insight into the adsorption kinetics models for the removal of contaminants from aqueous solutions, J. Taiwan Inst. Chem. Eng., 74 (2017) 25–48.
[63] N. Ouasfi, M. Zbair, S. Bouzikri, Z. Anfar, M. Bensitel, H. Ait Ahsaine, E. Sabbard, L. Khamliche, Selected pharmaceuticals removal using algae derived porous carbon: experimental, modeling and DFT theoretical insights, RSC Adv., 9 (2019) 9792–9808.
[64] C.P. Amézquita-Marroquín, P. Torres-Lozada, L. Giraldo, P.D. Húmpola, E. Rivero, P.S. Poon, J. Matos, J.C. Moreno-Piraján, Sustainable production of nanoporous carbons: kinetics and equilibrium studies in the removal of atrazine, J. Colloid Interface Sci., 562 (2020) 252–267.
[65] R. George, S. Sugunan, Kinetics of adsorption of lipase onto different mesoporous materials: evaluation of Avrami model and leaching studies, J. Mol. Catal. B: Enzym., 105 (2014) 26–32.
[66] S.M. Abdel Azeem, S.M. Mohamed Attaf, M.F. El-Shahat, Acetylacetone phenylhydrazone functionalized polyurethane foam: determination of copper, zinc and manganese in environmental samples and pharmaceutics using flame atomic absorption spectrometry, React. Funct. Polym., 73 (2013) 182–191.
[67] Z.M. Saigl, Sorption behavior of selected chlorophenols onto polyurethane foam treated with iron(III): kinetics and thermodynamic study, Environ. Monit. Assess., 192 (2020) 748, doi: 10.1007/s10661-020-08693-5.
[68] H. Qiu, L. Lv, B.-c. Pan, Q.-j. Zhang, W.-m. Zhang, Q.-x. Zhang, Critical review in adsorption kinetic models, J. Zhejiang Univ. Sci. A, 10 (2009) 716–724.
[69] S. Dawood, T.K. Sen, Removal of anionic dye Congo red from aqueous solution by raw pine and acid-treated pinecone powder as adsorbent: equilibrium, thermodynamic, kinetics, mechanism and process design, Water Res., 46 (2012) 1933–1946.
[70] K.U. Ahamad, R. Singh, I. Baruah, H. Choudhury, M.R. Sharma, Equilibrium and kinetics modeling of fluoride adsorption onto activated alumina, alum and brick powder, Groundwater Sustainable Dev., 7 (2018) 452–458.
[71] H.M. Al-Saidi, M.S. El-Shahawi, An innovative platform exploiting solid microcrystalline cellulose for selective separation of bromate species in drinking water: preparation, characterization, kinetics and thermodynamic study, Microchem. J., 159 (2020) 105510, doi: 10.1016/j.microc.2020.105510.
[72] L.A. Zambrano-Intriago, M.L. Gorozabel-Mendoza, A.C. Mosquera, M.H. Delgado-Demera, M.M.M. Bezerra Duarte, J.M. Rodríguez-Díaz, Kinetics, equilibrium, and thermodynamics of the blue 19 dye adsorption process using residual biomass attained from rice cultivation, Biomass Convers. Biorefin., 12 (2020) 3843–3855.
[73] A.R. Cestari, E.F.S. Vieira, A.A. Pinto, E.C.N. Lopes, Multistep adsorption of anionic dyes on silica/chitosan hybrid: 1. Comparative kinetic data from liquid- and solid-phase models, J. Colloid Interface Sci., 292 (2005) 363–372.
[74] C. Yao, C. Zhu, A new multi-mechanism adsorption kinetic model and its relation to mass transfer coefficients, Surf. Interfaces, 26 (2021) 101422, doi: 10.1016/j.surfin.2021.101422.
[75] A.A. Bhatti, S. Memon, N. Memon, A. Bhatti, B. Solangi, Evaluation of chromium(VI) sorption efficiency of modified Amberlite XAD-4 resin, Arabian J. Chem., 10 (2013) 1111–1118.
[76] B.H. Hameed, M.I. El-Khaiary, Equilibrium, kinetics and mechanism of malachite green adsorption on activated carbon prepared from bamboo by K_2CO_3 activation and subsequent gasification with CO_2, J. Hazard. Mater., 157 (2008) 344–351.
[77] F. Xiong, B. Hwang, Z. Jiang, D. James, H. Lu, J. Moortgat, Kinetic emission of shale gas in saline water: Insights from experimental observation of gas shale in canister desorption testing, Fuel, 300 (2021) 121006, doi: 10.1016/j.fuel.2021.121006.
[78] E. Abdelillah, A. Elhussein, S. Şahin, Ş. Sena Bayazit, Preparation of CeO_2 nanofibers derived from Ce-BTC metal-organic frameworks and its application on pesticide adsorption, J. Mol. Liq., 255 (2018) 10–17.
[79] M.A. Al-Ghouti, D.A. Da'ana, Guidelines for the use and interpretation of adsorption isotherm models: a review, J. Hazard. Mater., 393 (2020) 122383, doi: 10.1016/j.jhazmat.2020.122383.
[80] K.Y. Foo, B.H. Hameed, Insights into the modeling of adsorption isotherm systems, Chem. Eng. J., 156 (2010) 2–10.
[81] W.Y. Cheng, N. Li, Y.Z. Pan, L.H. Jin, The adsorption of Rhodamine B in water by modified zeolites, Mod. Appl. Sci., 10 (2016) 67, doi: 10.5539/mas.v10n5p67.
[82] J. Shah, M. Rasul Jan, A. Haq, Y. Khan, Removal of Rhodamine B from aqueous solutions and wastewater by walnut shells: kinetics, equilibrium and thermodynamics studies, Front. Chem. Sci. Eng., 7 (2013) 428–436.
[83] R. Jain, M. Mathur, S. Sikarwar, A. Mittal, Removal of the hazardous dye Rhodamine B through photocatalytic and adsorption treatments, J. Environ. Manage., 85 (2007) 956–964.
[84] M.N. Sahmoune, Evaluation of thermodynamic parameters for adsorption of heavy metals by green adsorbents, Environ. Chem. Lett., 17 (2019) 697–704.

[85] H.N. Tran, S.-J. You, H.-P. Chao, Thermodynamic parameters of cadmium adsorption onto orange peel calculated from various methods: a comparison study, J. Environ. Chem. Eng., 4 (2016) 2671–2682.
[86] S. Chen, C. Qin, T. Wang, F. Chen, X. Li, H. Hou, M. Zhou, Study on the adsorption of dyestuffs with different properties by sludge-rice husk biochar: adsorption capacity, isotherm, kinetic, thermodynamics and mechanism, J. Mol. Liq., 285 (2019) 62–74.
[87] S. Fan, Y. Wang, Z. Wang, J. Tang, J. Tang, X. Li, Removal of methylene blue from aqueous solution by sewage sludge-derived biochar: adsorption kinetics, equilibrium, thermodynamics and mechanism, J. Environ. Chem. Eng., 5 (2017) 601–611.